Renewable Energy 128 (2018) 324–336

Contents lists available at ScienceDirect

Renewable Energy

journal homepage: www.elsevier.com/locate/renene

Wind power characteristics of Oahu, Hawaii

D. Argüeso[*, 1], S. Businger

Department of Atmospheric Sciences, University of Hawai'i at Mānoa, 2525 Correa Rd. HIG350, 96822 Honolulu, HI, USA

ARTICLE INFO

Article history:
Received 6 April 2017
Received in revised form
27 March 2018
Accepted 21 May 2018
Available online 23 May 2018

Keywords:
Wind energy
Regional atmospheric modeling
Climate modeling
Wind-power potential
WRF

ABSTRACT

Renewable energy is a main avenue to reduce greenhouse gas emissions and mitigate climate change, as well as health impacts, associated with mining, refining and burning fossil fuels. Isolated locations with consistent natural energy resources patterns, such as Hawaii, have great potential to reduce their dependence on fossil fuels and generate energy locally. Using a regional atmospheric model, we explored the wind-power potential of Oahu at high resolution (1 km) and over a period (2005–2014) that allowed the assessment of variability from hourly to interannual. A validation of the model using both weather stations and wind farms showed the need for observational data at the turbine hub height to correctly estimate model errors for wind power applications because the model response can be quite different at standard near-surface wind measurement heights. The model performance at larger timescales evidences the potential for long-term assessment of wind characteristics. On the other hand, the model errors at sub-daily timescales indicated limitations of short-term planning, except for sudden changes in wind speed, which were accurately simulated. Our results identify optimal locations for wind power plants from capacity factor estimates, which include analysis of mean, variability at different timescales, ramps, and sustained periods of low generation.

Published by Elsevier Ltd.

1. Introduction

In Hawaii, more than 80% of the electricity consumed in 2015 was sourced from petroleum (69.4%) and coal (13.2%) [1]. In addition to the environmental costs, Hawaii's remoteness and the disaggregation of island grids contribute to a substantial increase in the final user electricity price. In fact, Hawaii consistently had the highest prices for electricity and natural gas in the U.S [2]. However, Hawaii has a great potential for renewable energies such as solar, wave [3] and wind to be widely implemented, and the benefits of locally generating the energy will promote adoption of renewable energies elsewhere. Despite Hawaii's potential for both offshore and onshore wind power generation, wind only accounted for 6.1% of the electricity generated in 2015, although still above the national average of 4.7%.

Designing viable and cost-effective wind power infrastructures requires detailed assessment of wind power resources. Therefore, high-quality and comprehensive wind speed data are necessary to investigate characteristics of wind resources at multiple timescales, including the long-term variability (e.g., interannual) and rapid changes (e.g., sub-hourly) in wind speed. Data sets must encompass a long enough time period, at high temporal frequency, at the height of turbine hubs, and with fine spatial resolution and complete coverage. Unfortunately, such observational datasets are rarely available. Direct measurements of wind speed in prospective areas for wind power development are often insufficient or non-existent (i.e., offshore and remote land areas). Finally, observations that span multi-year periods are generally limited to a few standard variables at a reference height that varies between 2 and 10 m, which are not necessarily representative of the conditions at turbine hub heights. To overcome many of these obstacles and produce useful wind resource guidance, modeling approaches would be an interesting alternative to existing options.

High-resolution atmospheric models are powerful tools able to generate complete and physically consistent information for wind power assessments. They provide information at multiple levels above the ground that include not only wind speed and direction, but also many other variables that may be useful to assess the correct functioning of wind turbines (e.g., temperature, air density). Furthermore, regional models allow for wind energy estimates at typical turbine hub heights. In the recent past, this type of model

* Corresponding author.
E-mail addresses: dab8@hawaii.edu (D. Argüeso), businger@hawaii.edu (S. Businger).
[1] Present address: Dr. Daniel Argüeso, Edif. Antoni Maria Alcover i Sureda, Despacho 2, Physics Department, University of Balearic Islands, Cra de Valldemossa km 7.5 07122, Palma, Spain.

https://doi.org/10.1016/j.renene.2018.05.080
0960-1481/Published by Elsevier Ltd.

has been adopted to provide estimates of wind resources in Portugal [4], Greece [5], and Chile [6], to mention a few. Models were also used to investigate future projections of wind energy resources in Ireland [7] and South Africa [8]. Other researchers used ensembles of regional models to determine the future power potential of wind in Europe [9] and mainland USA [10]. Most of these studies were constrained by computational resources and models that were either run at relatively coarse resolution for wind purposes or over periods that rarely exceeded a year. For instance, previous research [11] provided maps of wind power potential for the Hawaiian archipelago using a regional model, but only for the year 2014. Although, these assessments are highly valuable, they do not provide data on the long-term variability and may lack statistical robustness.

In this study, we validate a regional climate model using both standard weather station data and data from wind farms to identify the model's limitations and determine its ability to produce realistic wind regimes from a wind energy perspective on Oahu. To that purpose, we performed high-resolution (1 km) simulation experiments over a 10-year period (2005–2014) and stored variables that are relevant for wind power at typical turbine hub heights and at high frequency. As a result, we provide an analysis of the wind characteristics of the island with wind power generation in mind and made some determinations regarding the strengths and limitations of the modeling system.

2. Methods

2.1. Atmospheric model and experiment design

In this study, the Weather Research and Forecasting (WRF) Model version 3.7.1 [12] was chosen to simulate the atmosphere of the Hawaiian island chain, with focus on the most populated island, Oahu. Previous studies have evaluated and successfully used the model to simulate the climate of the region [13,14]. Also, it has been satisfactorily applied to investigate near-surface wind characteristics [15–18], as well as wind power capabilities in a wide range of locations including both onshore and offshore areas [6,19,20].

The atmosphere of Hawaii was simulated over a period of 10 years (2005–2014) to generate statistically robust information on the region's wind characteristics. The European Centre for Medium-Range Weather Forecasting reanalysis data ERA-Interim [21] provided the initial and boundary conditions for the WRF model runs. The simulation was divided into 36-h experiments that included 12-h spin-up periods. After discarding the spin-up periods, each simulation contained 24 h of valid data and all simulations were concatenated to obtain the 10-year representation of the climate of Hawaii. To cover the 10-year period required considerable computational resources and the resulting raw data set comprised 3.7 terabytes of data.

Three nested model domains were used to represent the region. The inner domain resolves Oahu at 1-km resolution (the island is described by 1506 land grid points) and the outer domains cover a wide area of the Central Pacific and the Hawaii archipelago at 25 and 5 km, respectively (Fig. 1). Spectral nudging was applied to winds and geopotential height in the 25-km domain, above the planetary boundary layer only, and to waves greater than 500 km. Spectral nudging is aimed at lessening the effects of the domain design and preserving the large-scale information from the boundary conditions. The technique adjusts selected variables to the forcing data at large scales only using spectral decomposition, as opposed to traditional nudging that does not discriminate spatial scales. Thus, large systems are consistent in both the regional climate model and the forcing data, while fine details produced by the regional climate model are maintained. Further information on the technique can be found in Refs. [22] and [23]. High spatial resolution allows for detailed representation of the orography, which is crucial for wind power studies, especially given the complex topography of Oahu. The other two domains helped bridge the resolution difference between the boundary conditions and the fine-resolution domain, as well as optimize the computational resources.

The Yonsei University (YSU) Planetary Boundary Layer (PBL) scheme [24] was chosen to represent the turbulence in the lower atmosphere because it includes an option to improve the influence of topography on near-surface winds [17]. The WRF Single-Moment 6-Class Microphysics (WSM-6) scheme [25] was chosen following Zhang et al. (2012) [13] to include cloud microphysics processes in the model. The Rapid Radiative Transfer Model (RRTM) for longwave radiation and the Dudhia scheme for shortwave radiation were selected due to their efficiency and proven good performance for wind resources studies in multiple regions across the globe [4,5,16,26,27]. Convective processes were represented with the Betts-Miller-Janjic (BMJ) cumulus scheme in the outer domains, while it was switched off in the 1-km domain because it was assumed that most of the convective circulation is explicitly resolved. The land-atmosphere interactions were simulated using the Noah Land Surface Model [28].

The standard model outputs were saved at 3-hourly intervals, but the standard meteorological variables and additional variables relevant for wind and solar energy applications were saved every hour. The model code was modified to compute and save wind speed and wind power density—as well as solar energy variables—at different typical turbine hub heights (i.e., 80, 100, 120 and 150 m above ground level). Additionally, statistics such as the mean, maximum, and standard deviation were calculated over all time steps and saved every 15 min for several variables, including multiple-height wind speed and wind power density. This constitutes the most detailed information of wind and solar energy resources in Oahu available to date both in terms of its spatial and temporal resolution and coverage.

2.2. Observational data

The suitability of the model to investigate Oahu's wind resources was determined through model validation with *in situ* observations. Fig. 1b shows the location of the stations used in this study, including four from the U.S. National Weather Service (NWS) network and three stations from the U.S. Remote Automated Weather Stations (RAWS) network. All selected stations contained at least 80% of valid hourly data over the simulated period (2005–2014). The model near-surface wind speed was directly compared to NWS stations because both include data measured 10 m above the ground. It should be noted that some NWS stations had a minimum wind speed sensitivity of 1.544 m s^{-1} (3 knots), thus all model wind speeds below that threshold were set to 0 m s^{-1}. RAWS anemometers are located at 6.1 m above the ground and thus the model output needed to be extrapolated to that height. Such conversion was made using a simple wind profile power law [29] assuming neutral stability conditions ($\alpha = 1/7$), which is a commonly used approach in wind power studies [19,20,30,31].

In addition, the model is evaluated at the turbine hub height using wind power generation data from two wind farms located in Kahuku and Kawailoa, both on Oahu (Fig. 1). In both cases the hub height was 80 m. The information provided was gross generation as derived from wind speed using power conversion curves. Kahuku has 2.5 years of data (2012–2014), while Kawailoa has only one year (2013). Kahuku turbines are Clipper Liberty 2.5 and Kawailoa turbines are Siemens 2.3–101, which are classified as classes IEC-3

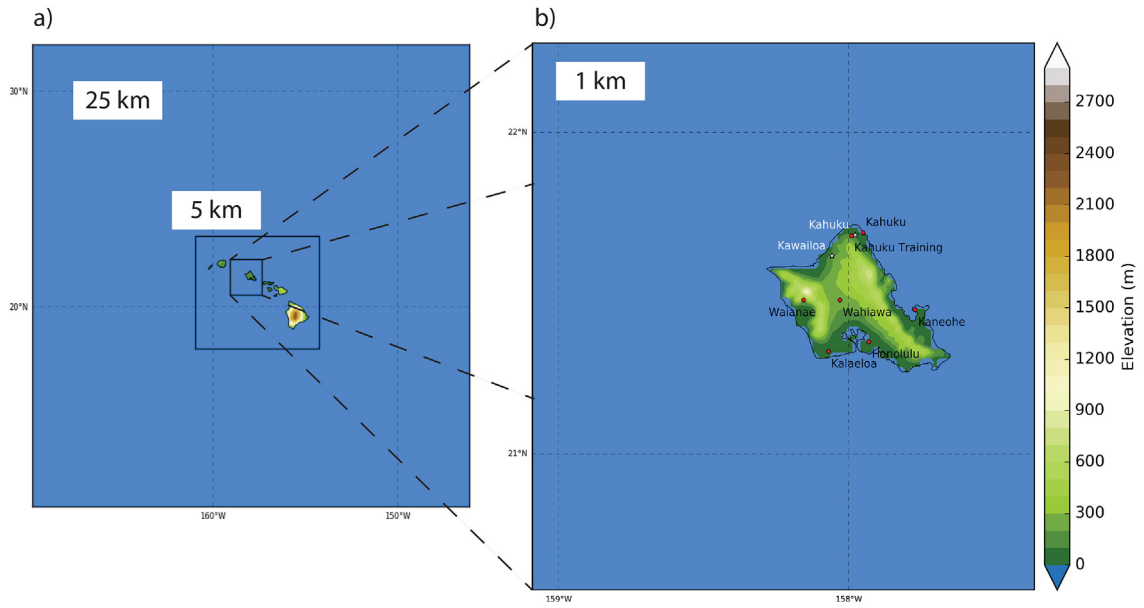

Fig. 1. (a) Location, extent and resolution of the model domains and (b) map of the finest resolution domain and the location of NWS and RAWS observational sites (red circles), wind farms (white stars). The 1-km resolution domain has 181 by 191 grid points and 40 vertical levels. (For interpretation of the references to colour in this figure legend, the reader is referred to the Web version of this article.)

and IEC-2, respectively. Kahuku has 30 MW installed and Kawailoa has 69 MW. The empirical power curves to convert from simulated wind speed to simulated wind power (Supplementary Fig. 1) in this study were obtained from the U.S. National Renewable Energy Laboratory [32].

3. Results and discussion

3.1. Wind speed validation

We evaluated three different aspects of the model performance in representing wind speed characteristics at weather stations: probability distribution function; diurnal cycle; and seasonal cycle. Other evaluation metrics are also often used in the literature such as the Weibull parameter comparison [20,33]. To facilitate comparison with existing studies, we included the Weibull fitting validation in the supplementary material (Supplementary Table 1 and Supplementary Fig. 2). While wind direction may also be important from a wind power perspective, wind regimes in Hawaii are dominated by persistent northeast trades, especially during summer months. On Oahu, southerly wind components are not only rare, but also generally weak [30]. Therefore, our study focuses on wind speed and its variability.

Fig. 2 shows the seasonal cycle of wind speed in seven different locations (Fig. 1) from station measurements and the model (nearest land grid point to each station). In all cases the model represents the shape of the seasonal cycle accurately, with differences that are mostly constant throughout the year and thus explained by biases specific to each location. In Honolulu (PHNL) and the northern stations near Kahuku (KTAH1 and KFWH1), the model systematically underestimates the observed wind speeds, although the largest differences are within 30% of the observed values (Fig. 2a–c). In protected areas in the interior of the island such as Wahiawa (PHHI) and Waianae (WNVH1), the model does a remarkable job at simulating the relatively flat seasonal cycle of wind speeds with values close to 3 m s^{-1} and errors that remain within 10% of the observed values (Fig. 2d–e). In southern exposed stations Kalaeloa (PHJR) and Kaneohe (PHNG), the model overestimates 10 m wind speeds by up to 90% in summer (Fig. 2f–g). It is worth noting the model ability to represent the local minimum in May, a feature shared by all locations. Also, the persistence of stronger winds during summer due to the dominance of trades is well represented in the model, except perhaps for stations where the model overestimates wind speed. In these stations, the simulated seasonality is too strong compared to the observations.

Regarding the diurnal cycle (Fig. 3), all locations are characterized by a maximum in the central hours of the day, especially in Honolulu, Wahiawa and Kalaeloa. The model replicates the shape of the diurnal cycle in all locations except for Waianae (WNVH1) where the wind tends to pick up again at night, which is probably influenced by a mountain-valley circulation. The model reproduces this second maximum well, but misses the main maximum in the middle of the day. The differences between modeled and observed diurnal cycles are consistent with the biases in the seasonal cycle. For instance, WRF underestimates wind speed throughout the day in both stations near Kahuku by 1–2 m s^{-1} (20%–35% of observations), and at night in Honolulu by 1–1.5 m s^{-1} (~40% of observations), while matching the observed values very well in the late morning. In Waianae and Wahiawa, the model produces a slightly weaker diurnal cycle than observations, but the differences do not exceed 1 m s^{-1} at any time of the day. On the other hand, WRF overestimates hourly values by 1.5–2.0 m s^{-1} in Kaneohe and Kalaeloa, which at night could represent almost 100% of the observed values. The timing of the diurnal cycle is very accurate in the model and changes in the model wind speed occur within 1 h of changes in the observations. Note that measurements and WRF times could indeed differ up to an hour because observations were rarely taken exactly at the hour.

In stations where WRF underestimated wind speed, the PDFs and the q-q plots reveal that the model produces too many moderate wind events (2–5 m s^{-1}), while intense winds (>6 m s^{-1}) are systematically underestimated (Fig. 4a–c), especially in the two stations at the northeast (Kahuku Training and Kahuku). In Honolulu, there is a better agreement between the modeled and the observed percentiles, with differences smaller than 1 m s^{-1} for the

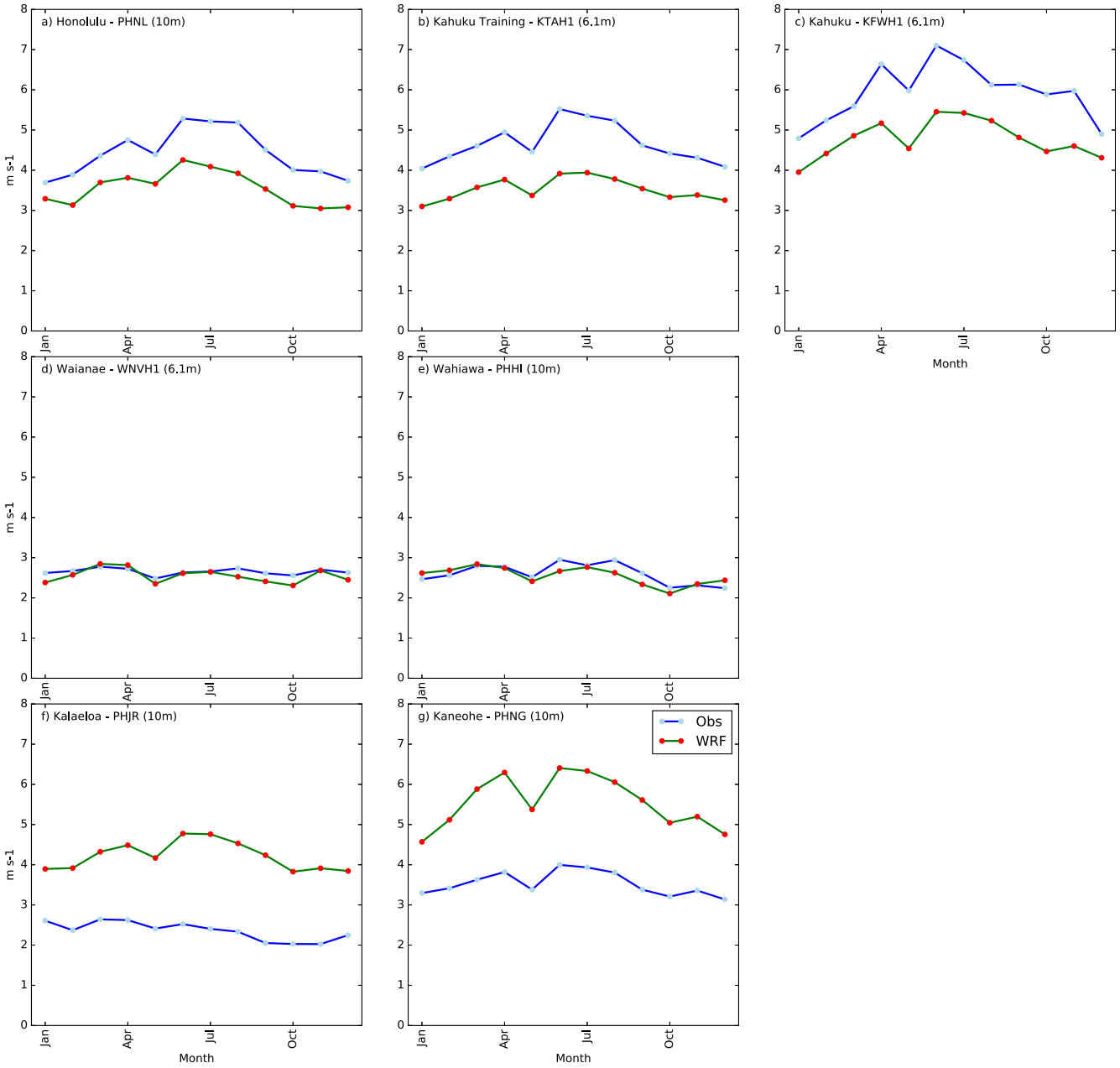

Fig. 2. Seasonal cycle of monthly average wind speed in seven different locations on Oahu (Fig. 1) from NWS and RAWS stations (blue) and WRF model (green/red). (For interpretation of the references to colour in this figure legend, the reader is referred to the Web version of this article.)

highest percentiles (>90th) and larger in the interquartile range (25th-75th). The model tends to underestimate wind speeds as suggested by the q-q plot and the PDFs, which shows more simulated hours with wind speeds in the range 1.5–3 m s^{-1} and fewer with wind speeds above 4 m s^{-1} than in the observations. Wind speed distributions in Waianae and Wahiawa are very well simulated by the model. In Waianae, the simulated distribution is slightly wider than observed, thus the model overestimates the occurrence of both light and strong winds, while the opposite occurs in the upper-tail of Wahiawa distribution. In both stations, the q-q plots show the close match between model and observations, with noteworthy differences only in the highest percentiles in Wahiawa (<2 m s^{-1} in the 99th percentile). In Kalaeloa and Kaneohe, the simulated distribution is substantially shifted towards higher values than the observed distribution, which is also reflected in an overestimation of most percentiles. This error becomes larger at the 90th percentiles, where the model is producing values that exceed observations by ~3 m s^{-1} (Fig. 4f–g). This is especially true for Kaneohe, where WRF often produces wind speeds ≥10 m s^{-1} (3.6%), which are very unlikely in the records for that period (0.20%).

Different systematic deviations of model wind estimates from observations at different locations in a confined area are likely caused by local factors that modulate the large scale flow at local scales. Possible sources of error may be related to the Planetary Boundary Layer parameterization or the neutral stability assumption used to calculate wind speed at different heights. They may also include, but are not limited to, misrepresentation of factors such as very fine topography (both orography and coastlines), sharp variations in aero-dynamical characteristics (i.e., roughness length)

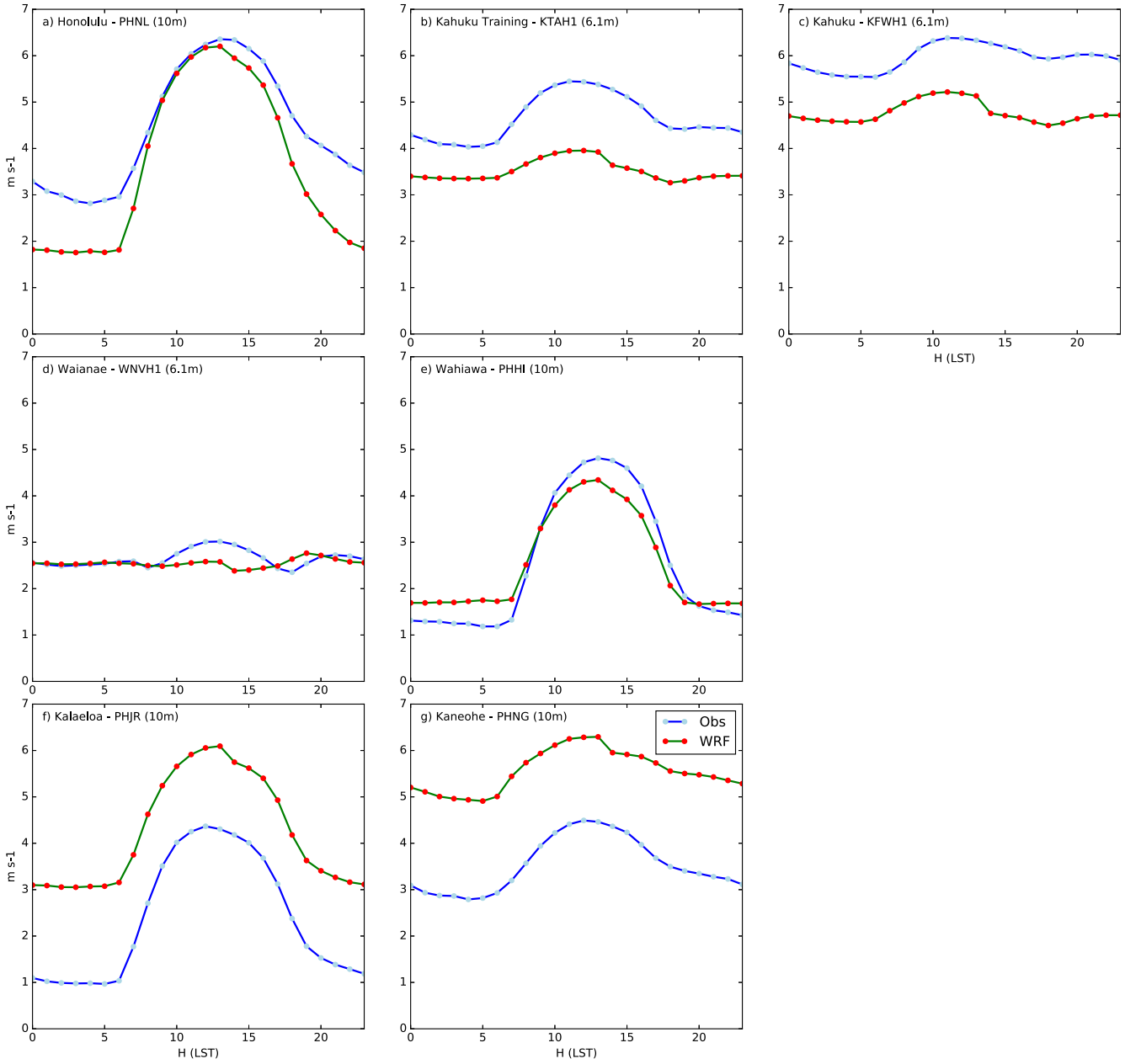

Fig. 3. Diurnal cycle of hourly wind speeds at seven different locations on Oahu (Fig. 1) from NWS and RAWS stations (blue) and WRF model (green/red). (For interpretation of the references to colour in this figure legend, the reader is referred to the Web version of this article.)

due to land-use heterogeneities, soil state (temperature and humidity), and sea-surface temperature. However, it should be noted that the influence of these factors is less pronounced at typical hub heights (80 m) than standard wind speed measurement heights (6.1 and 10 m).

These results suggest the utility of WRF to generate comprehensive information that can assist in the identification and characterization of potential wind farm locations. However, they also clarify the caveats that need to be considered when interpreting the wind power estimates from model outputs on Oahu, such as those associated with systematic biases in wind speeds. These uncertainties can be further reduced by a different parameterization scheme choice, particularly PBL, improvement of land use description, and greater model spatial resolution to better resolve topography.

3.2. Wind power validation

In addition to the comparison with near-surface measurements, we conducted a validation using wind power generation data, expressed as the capacity factor, from two wind farms on Oahu: Kahuku and Kawailoa (Fig. 1b). The capacity factor of a power plant is the ratio of its actual wind power generated over a period of time, to its maximum potential output assuming it could operate at full installed power over the same period of time. We estimated the wind power generated by the plant using empirical power curves that convert wind speeds into energy outputs (see Section 2.2). The capacity factor makes the wind resource results independent of the wind farm dimensions and enables direct comparison across plants. It also allows for scaling of the wind resource based on the capacity of prospective wind farms in future development plans.

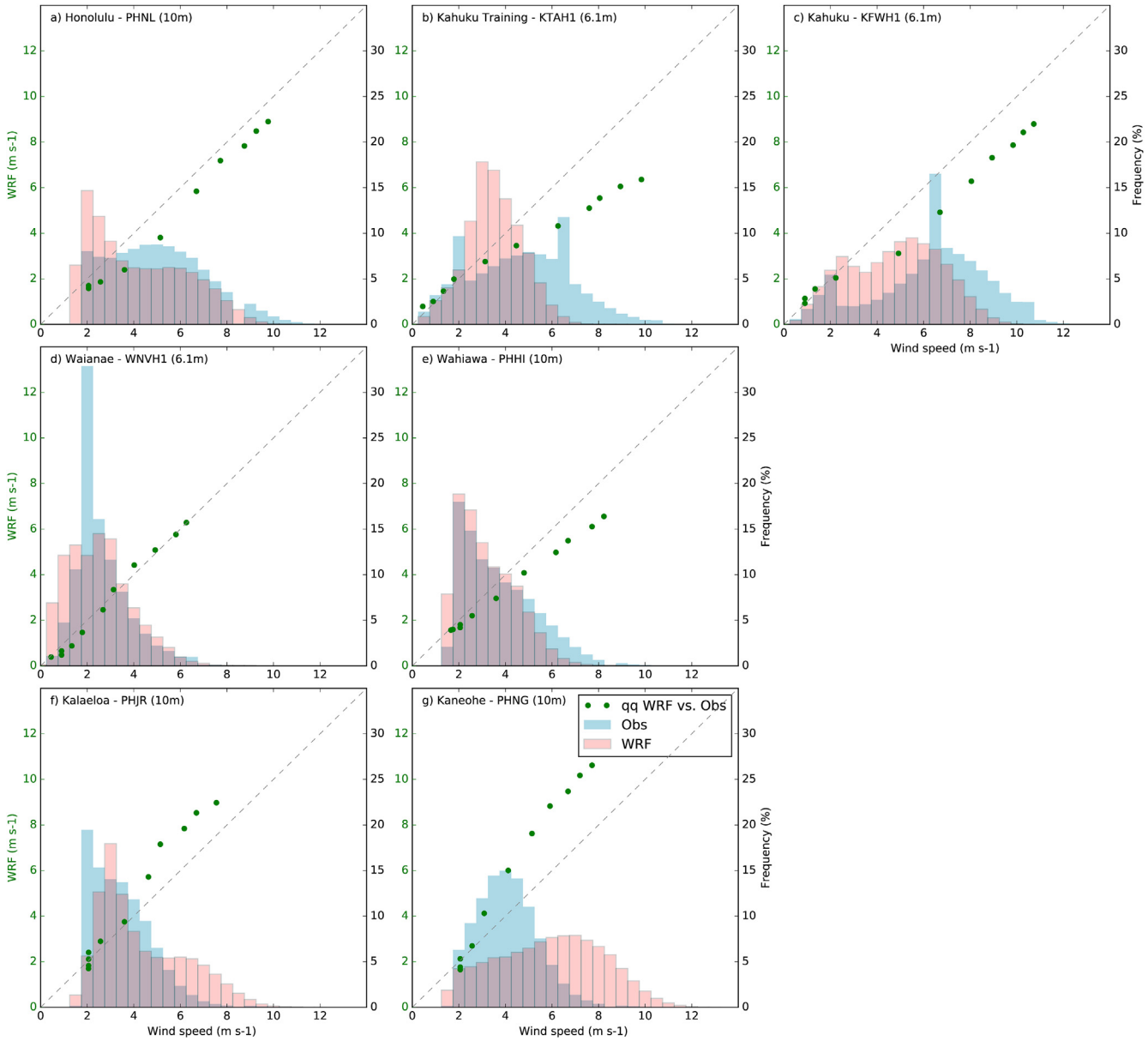

Fig. 4. Quantile-quantile plot of hourly near-surface wind speeds from WRF vs. observations (left y-axis, green circles). Percentiles represented by each circle are: 1st, 2nd, 5th, 10th, 25th, 50th, 75th, 90th, 95th, 98th, 99th. Diagonal dashed line represents a perfect agreement between model and observations. Bars are histograms of the probability distribution function (right y-axis) of near-surface wind speed from observations (blue) and the model (red). (For interpretation of the references to colour in this figure legend, the reader is referred to the Web version of this article.)

This validation helps determine the model performance in terms of wind power generation using typical turbine hub height wind speeds (80 m in the case of these two wind farms) and empirical wind-power conversion curves [28]. Because wind farms may extend over multiple model grid points, we selected all grid points that overlapped with the wind farm area to make the comparison (1 grid point for Kahuku and 10 grid points for Kawailoa; a single grid point comparison was also analyzed for Kawailoa without significant impact on the results).

From a seasonal perspective, WRF overestimates the observed monthly wind power capacity factor at 80 m above the ground level throughout the year in Kahuku (Fig. 5), which contrasts with the lower simulated wind speeds at 10 m (Fig. 3 b–c). This emphasizes the importance of evaluating the model not only at standard anemometer heights, but also at specific turbine hub heights. The difference is similar throughout the year and in the range 0.1–0.2. Thus, the shape of the seasonal cycle for these two years is very well represented in the model, with two major peaks in February and June, and significantly lower values between October and January. In Kawailoa, the simulated and observed values are much closer to each other, with larger differences (0.1) occurring mostly in the summer months (May–Aug.). Although the model also produces the peak in February and June, the two curves not as similar as in Kahuku. Nonetheless, caution must be used in interpreting these results because they only cover one year of data.

From a wind generation perspective, daily variability is also important. In this context, daily variability is defined using the Interquartile Range (IQR, q75-q25) of daily values. In Kahuku, the model tends to produce larger variability than observed, especially during the colder months when it can be twice that observed

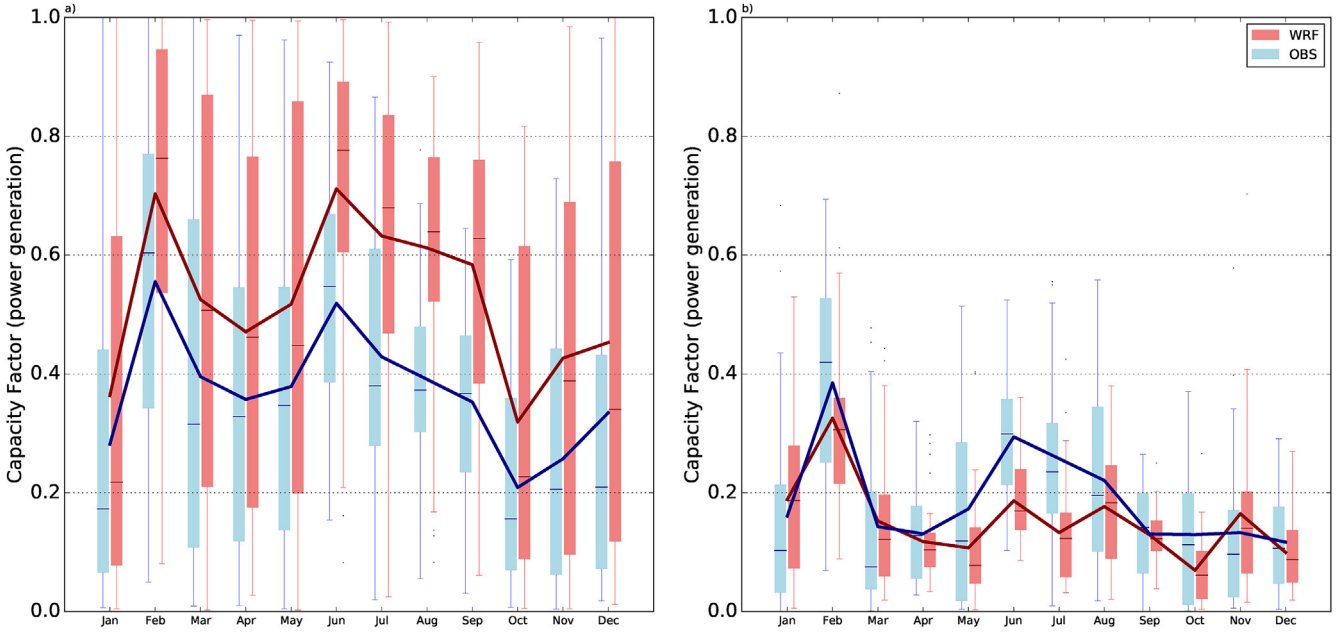

Fig. 5. Seasonal cycle of observed (blue) and simulated (red) wind power capacity factor at (a) Kahuku for 2012–2013 and (b) Kawailoa for 2013. Lines denote the monthly mean, boxes the interquartile ranges (IQR) of daily values, horizontal lines the medians of daily values, whiskers the ±1.5 IQR of daily values, and dots the outliers. (For interpretation of the references to colour in this figure legend, the reader is referred to the Web version of this article.)

(Fig. 5a). In summer months, simulated and observed variability are comparable, although the model overestimates capacity factor. In Kawailoa (Fig. 5b), modeled daily variability of the capacity factor is similar or smaller than observed but this is only for 2013, which is when observations where available, so these results should be regarded with caution.

Overall, WRF produces an accurate diurnal cycle in Kawailoa (Fig. 6b). In the early hours of the day, WRF variability is also similar to the observed with only minor differences (~10%). Later in the day, WRF produces smaller capacity factors than observed (0.1 at 14H) as well as reduced variability in the central hours of the day (~30% smaller). Observations and model capacity factors start to converge again in the late evening, although the observed variability remains larger (10–20%).

In Kahuku (Fig. 6a), WRF substantially overestimates both mean and variability of the observed hourly capacity factors throughout the day. Mean values are 0.1–0.2 larger in the simulations, while variability in the model is up to ~80% larger than the observed (13H). The drop in simulated wind energy production between 13H and 14H is a result of the experiment design. Even though a spin up

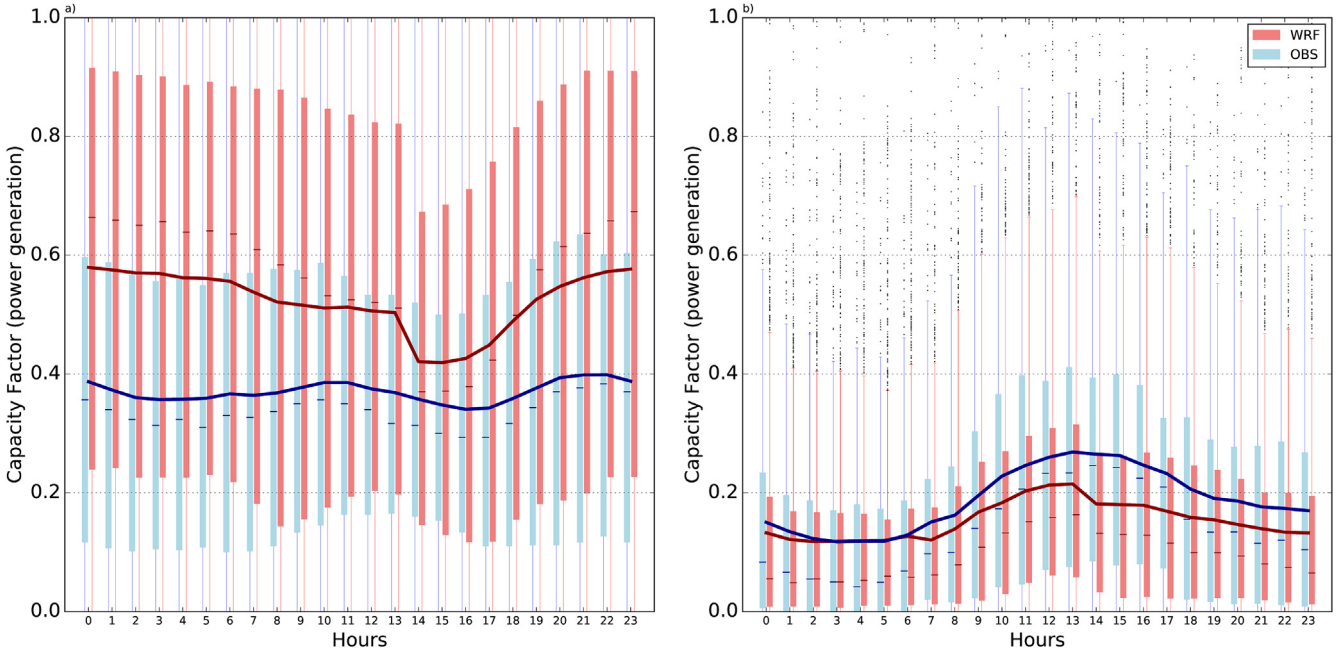

Fig. 6. Same as in Fig. 5 but for the diurnal cycle. Hours are in local time.

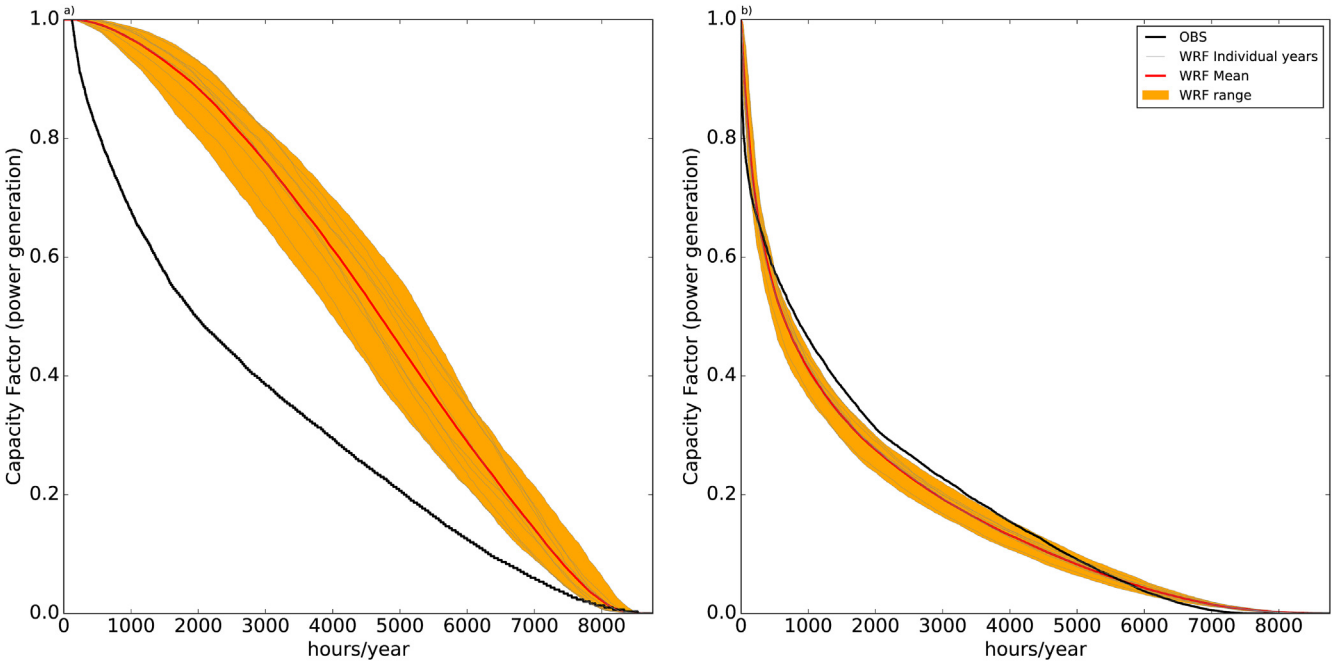

Fig. 7. Mean speed-duration curves of capacity factor from WRF (red) and observations (black) in (a) Kahuku and (b) Kawailoa. The entire simulated period (2005–2014) is shown for WRF and available records are shown for observations (2012–2013 for Kahuku and 2013 for Kawailoa). Grey lines represent individual simulated years and shading (yellow) represents the range of simulated values. (For interpretation of the references to colour in this figure legend, the reader is referred to the Web version of this article.)

of 12H was adopted, the concatenation of individual simulations at 00H GMT (14H Local time) is apparent in the modeled capacity factor. We purposely chose this starting time so that most of the spin-up occurs at night, when winds are generally weaker. We also examined the impact of this choice by simulating 2013 using 00Z as the starting time and concatenating the runs at 12Z (02H Local time), and found that it indeed has a significant impact on the model performance (Supplementary Figs. 3 and 4) with our choice providing better results. However, this is not an unequivocal proof that the selected starting time is optimal. If greater computational resources are available in the future, longer simulations may be advisable to reduce this discontinuity. Bearing in mind this artifact, the simulated evolution of the capacity factor throughout the day provides reasonable guidance for planners.

The frequency in hours of a given capacity factor measures the wind power generation potential of a location and may be

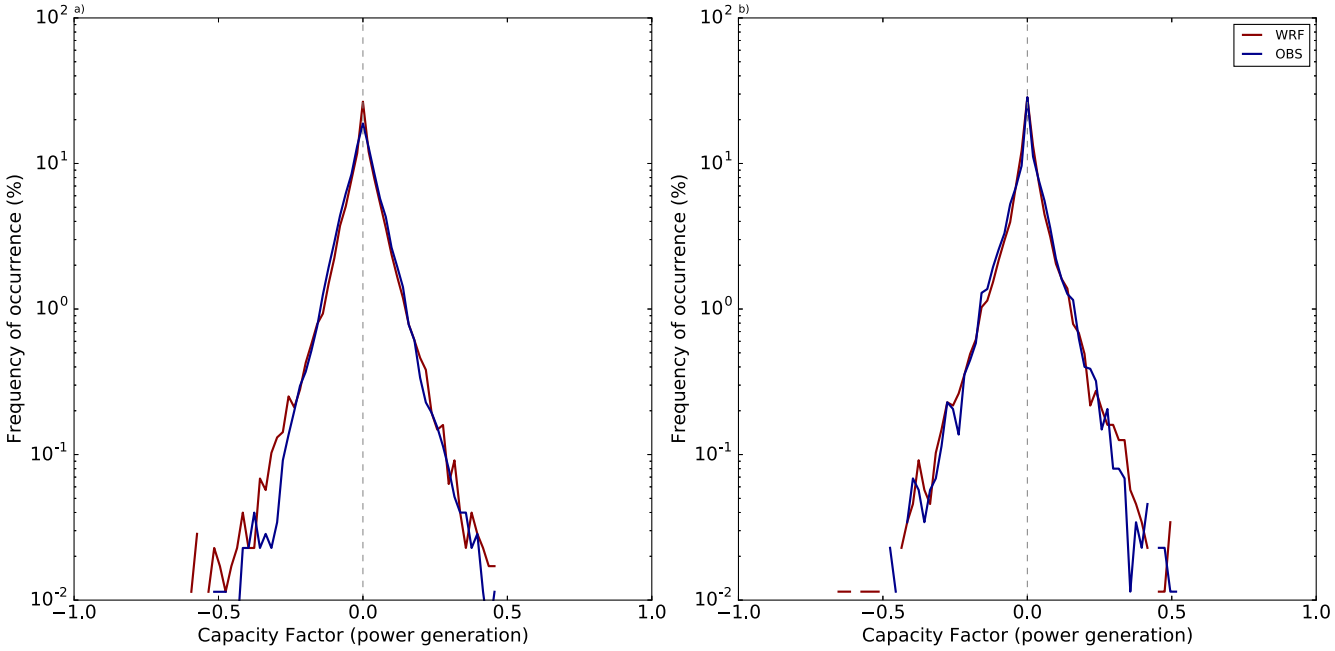

Fig. 8. Probability distribution function of hourly normalized (capacity factor) wind power ramps from observations (blue) and WRF (red) in (a) Kahuku and (b) Kawailoa during the observational period (2012–2013 for Kahuku and 2013 for Kawailoa). (For interpretation of the references to colour in this figure legend, the reader is referred to the Web version of this article.)

represented through the speed-duration curves (Fig. 7). While the model produces too many favorable conditions as compared to the observations in the windward station (Kahuku, Fig. 7a), the agreement between observations and model in Kawailoa (Fig. 7b) is very good. In Kahuku, the model predicts that, on average, the capacity factor will be at least 0.5 approximately 4700 h/year, which clearly overestimates the observed value of ~2000 h/year in 2012–2013. In Kawailoa, observed and modeled estimates are more modest and consistent: the 0.5 capacity factor threshold is only reached 800 h/year in the observations and 600 h/year in the model, while 3900 h/year the wind energy production factor was below 0.1 in the observations and 4100 in the model.

The model's ability to reproduce sudden changes in wind speed (ramps) must be evaluated because it has a significant impact on the wind plants operability. Despite the biases in wind power generation detected before, WRF provides an accurate estimate of the probability of sudden capacity factor changes in both locations, especially in Kawailoa (Fig. 8b). In Kahuku, the frequency of considerable drops in capacity factor (>0.25) is overestimated, although both in the observations and the model their frequency is approximately 0.1%.

3.3. Wind power resources in Oahu

The largest average capacity factor over the ten-year simulated period (2005–2014) is concentrated in the two main ridges, especially along the Koʻolau range in east Oahu, where mean capacity factor are between 0.7 and 0.8 over relatively large areas. However, these areas are generally of limited access because of the very complex topography and therefore may not be suitable for wind power purposes. More accessible areas with high mean capacity factors (above 0.5) are located near Kaʻena point (northwest), Kahuku point (north), and around the southeast corner of Oahu. Mokapu peninsula (east) also shows large average capacity factor values, but comparison with near-surface observations (Kaneohe) suggests that the model may overestimate wind speed at this location and thus additional evaluation is needed. Low mean capacity factors (<0.2) were obtained for the region between the two mountain ranges in the interior of the island and areas on the west coast.

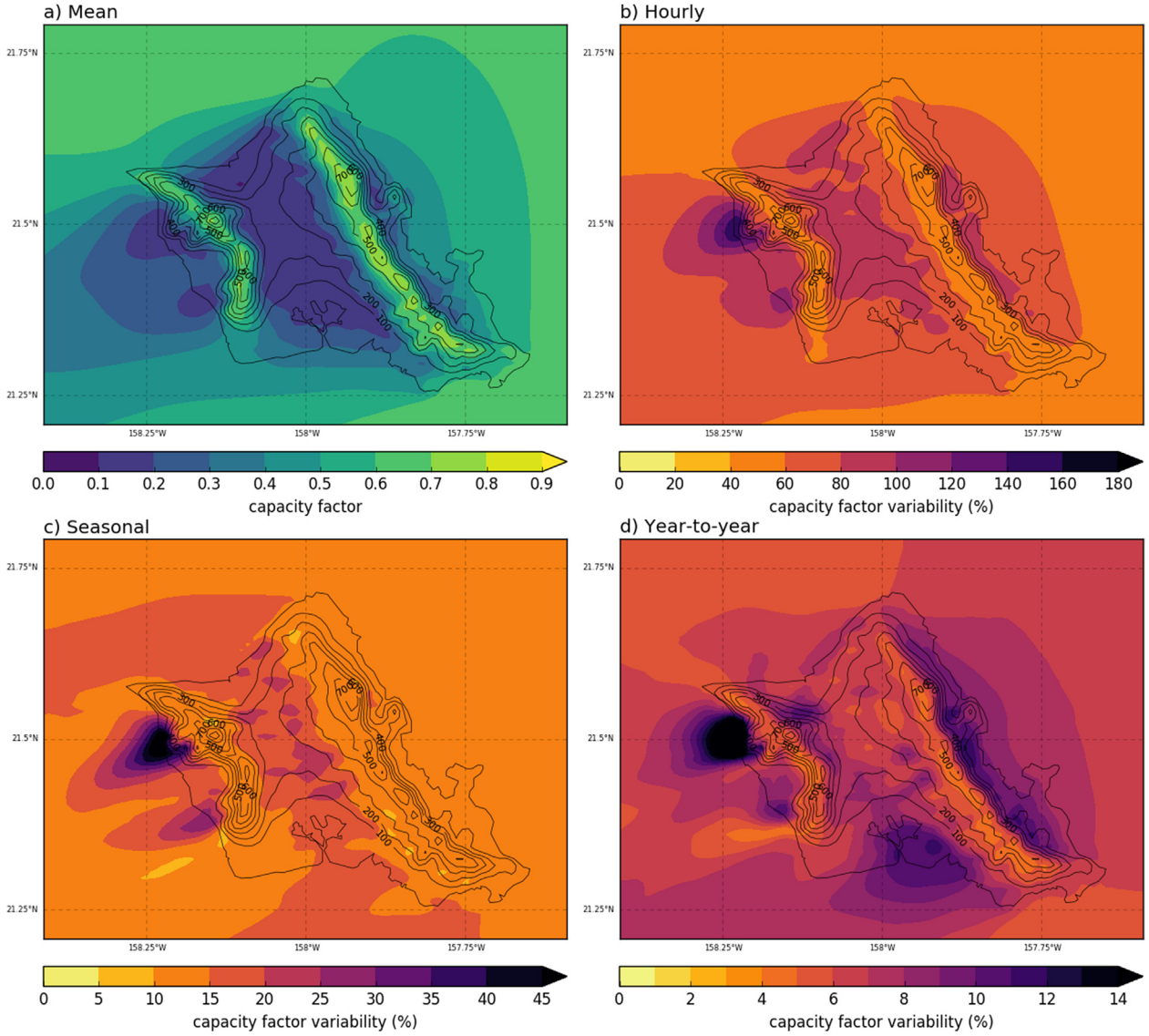

Fig. 9. Spatial distribution of (a) mean capacity factor and variability measured as normalized standard deviation of the (b) hourly, (c) monthly, and (d) annual mean capacity factor. The standard deviation of the monthly capacity factor was calculated using the average annual cycle. Elevation at 100-m intervals represented by black contours.

Variability of wind resources at different timescales is also a key factor in designing efficient wind power plants. Areas with high mean capacity factor values and low variability are generally preferred to provide consistent wind power generation. Fig. 9b shows the largest hourly variability, defined as the normalized standard deviation, over the west coast (as much as 140% of the average capacity factor), although this area has limited wind power potential, as indicated by the low mean capacity factors. The two ridges and four corners of the island show the lowest hourly variability with values between 20% and 40% of the mean capacity factor. Large areas of the island show values in the range 60%–80%, including Mokapu peninsula, mentioned previously. Such values may be acceptable because hourly variability includes aspects such as the diurnal and annual cycles, and at such scales wind resources may be subjected to large variations.

To narrow down this variability, we analyze the variability within the annual cycle (Fig. 9c). The mean capacity factor for each calendar month is calculated to create the annual cycle and the normalized standard deviation for these values was represented to account for typical seasonality in the island. This provides information on the potential of an area to produce consistent wind speed throughout the year. The largest seasonality occurs again along two sections of the west coast where the standard deviation of monthly averages exceeds 50% of the mean capacity factor. The most consistent regions occur near the two main mountain ridges and extend to lower elevation areas, which are more suitable for wind plants. For example, the southwest corner, leeward side of the Ko'olau range (east), and most of the eastern part of the island are characterized by seasonal capacity factor variability between 10% and 15% of the mean values.

Another important component of the variability from a planning point of view is the interannual variation. Year-to-year variability (Fig. 9d) is large (>10%) along the windward side of the Ko'olaus in east Oahu, parts of the west coast, and around Honolulu in the

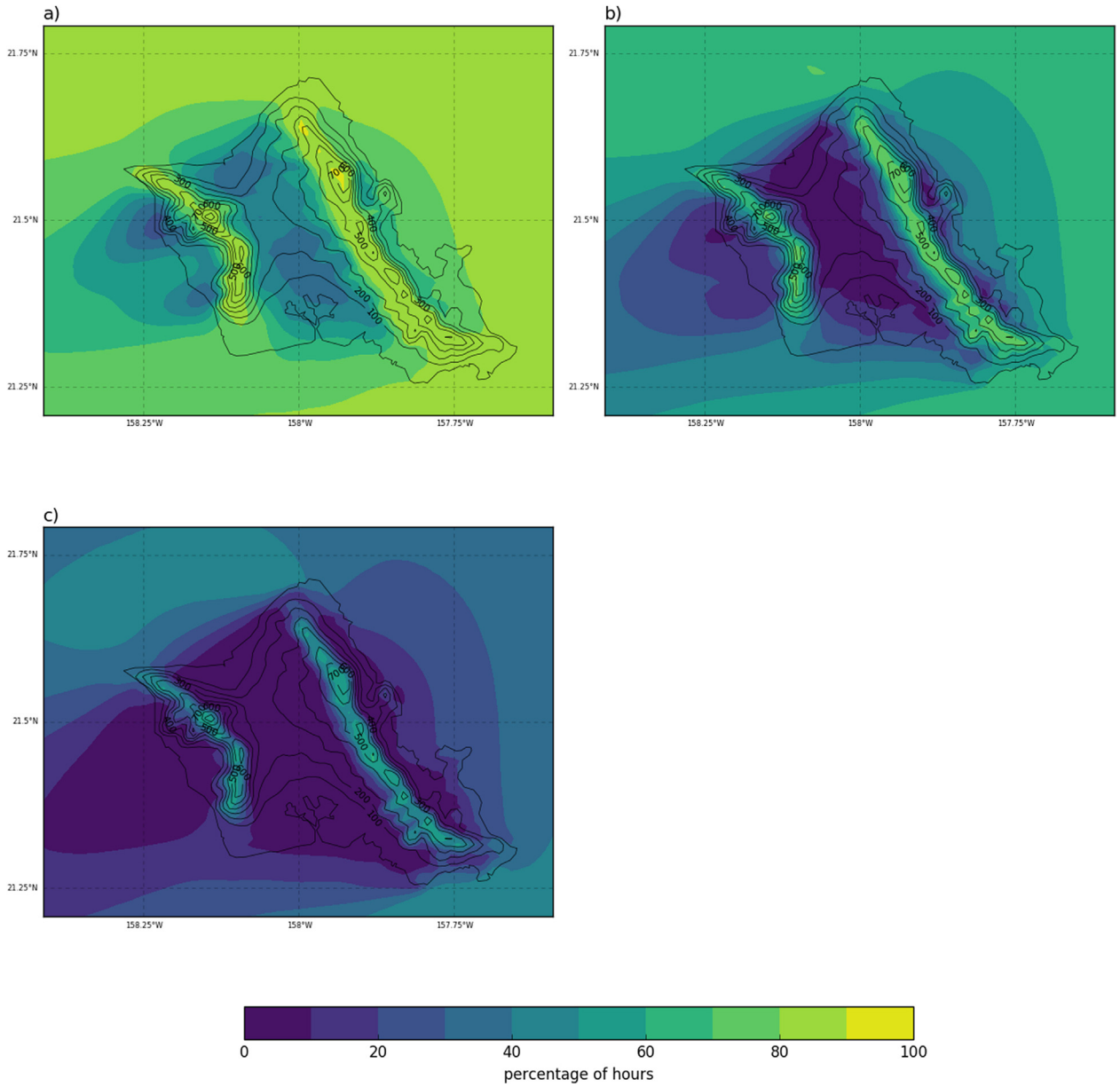

Fig. 10. Average percentage of hours with capacity factor above (a) 0.1, (b) 0.5, and (c) 0.9. Elevation at 100-m intervals represented by black contours.

south. Areas where interannual variability remains below 10% and showed low hourly and seasonal variability include the two mountain ranges and their leeward sides, as well as the four corners of the island. Parts of the interior of the island are also characterized by low interannual variability, but capacity factor values were generally too low in this region. Individual years may depart substantially (±20%) from the mean and thus the probability of years with anomalously low wind energy production should be taken into consideration.

The wind power potential of a location is often represented by the speed-duration curves as shown in Fig. 7. To allow for spatial examination of these curves, Fig. 10 shows the average percentage of hours with capacity factor above 0.1, 0.5 and 0.9. In accordance with previous results, areas of high wind power potential are co-located with topographical features. Areas with high capacity factors are in the four corners of the island and sections of the east coast. In these regions, the model indicates a potential of at least 0.5 during half of the hours, except in the southwest corner where such levels occur less often (>40% of hours). Hours of potential power generation close to the maximum plant capacity remain below 10% for most of the island, except for the previously mentioned regions where capacity factor values larger than 0.9 occur between 20 and 40% of the time. At higher elevations, the model also suggests frequencies above 50% for such capacity factor values. Large areas on the island are expected to produce some power (>0.1) at least 70% of the time, with substantially lower values (<40%) in the interior and the west coast.

Indeed, one of the factors that is crucial for wind energy planning is the occurrence of extended periods with very low power generation, when alternatives are required to replace wind resources. Fig. 11a shows the percentage of days with average capacity factor below 0.1. Only areas that were already identified as poor in terms of wind potential (interior and west coast), show large number of days (>40%) with low power generation. By contrast, locations that previously showed potential for wind power production (island corners, parts of east coast and leeward side of Ko'olau range), typically show 10%–20% of days with average capacity factor below 0.1. To determine how these days are clustered together in periods of low wind, Fig. 11b shows the percentage of days that contribute to sequences of three or more days with capacity factor lower than 0.1. In regions where low generation days were in the range 10%–20%, these periods account for less than 10% of the days, and even less than 5% in some cases, which would reduce the reliance on other sources of energy production to supply energy when wind speed is low. This study is focused on wind energy only, but the model outputs offer a unique opportunity to explore the correlation between solar and wind power resources, and thus investigate how they complement each other to plan for storage in such conditions.

4. Conclusions

In this study, we evaluated WRF for wind power applications using observational data from weather stations and wind farms. We also investigated the wind power characteristics of Oahu at multiple timescales, from hourly to interannual.

Our results emphasize the need to perform model validation using wind power generation or wind speed data at specific turbine hub heights in addition to standard anemometer heights. Otherwise, the model validation may provide misleading information due to contrasting model performance at different heights.

Unlike previous studies [5,11] (and references therein), a 10-year simulation was analyzed to determine the importance of long-term variability. We showed that interannual variability as measured by the normalized standard deviation is typically 10% of the average wind power generation, with extreme years departing significantly more from the mean (~20%). Also, areas where the mean capacity factor is appropriate to project wind farm development can be affected by large interannual variability, hence the need for longer assessment periods to consider this potential risk.

Overall, WRF does a good job of reproducing many of the observed characteristics such as the hourly quantiles or the seasonal cycle of wind speed. However, the model produces biases that need to be considered when planning potential wind energy plants. This is because in some cases it may indicate overly favorable wind power generation estimates (i.e., speed-duration curves, seasonal averages). The validation with wind farm data was limited to two locations and therefore it may be useful to extend this study to other locations to obtain a range of possible model responses, as shown by the comparison with weather stations.

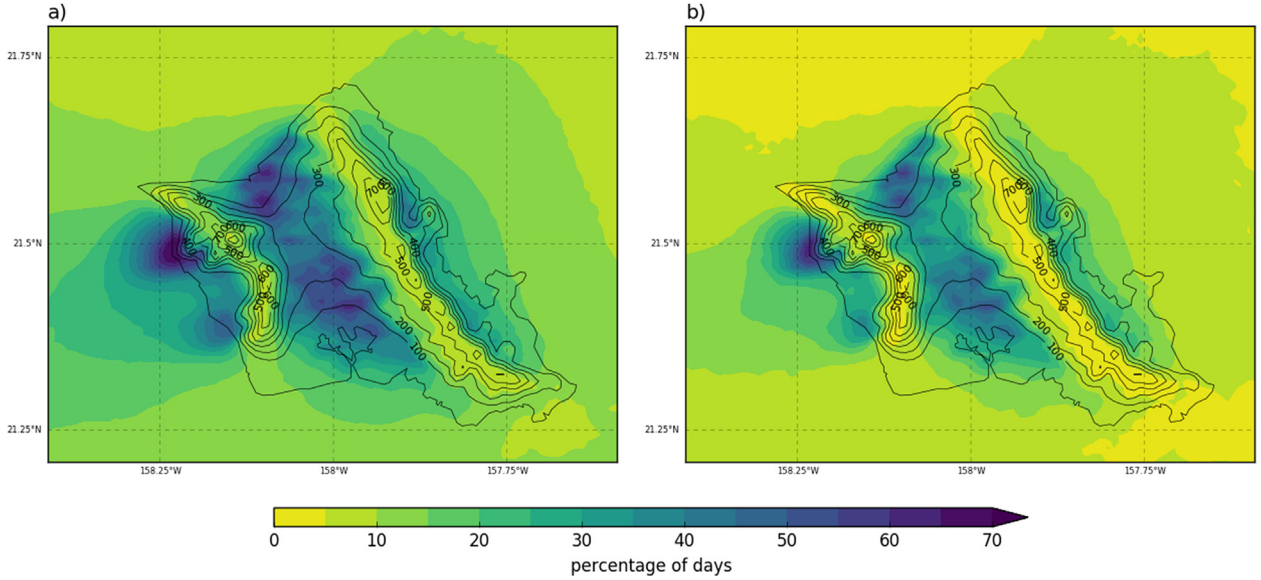

Fig. 11. (a) Average percentage of days with low power generation (daily mean capacity factor < 0.1) and (b) average percentage days that contribute to low power generation spells (periods of three or more days with mean daily capacity factor < 0.1). Elevation at 100-m intervals represented by black contours.

Long-term estimates of wind energy generation are reliable if biases are properly accounted for as evidenced by the seasonal cycle and monthly variability. However, planning for storage and production at higher frequencies (i.e., sub-daily) is more challenging because estimates may be less accurate and prone to non-negligible uncertainties. Nonetheless, the model accurately simulates the capacity factor ramps, which provide confidence in a crucial aspect of wind power assessment, such as the sudden drops and increases of wind power generation, even at hourly timescales.

According to the model, the areas with the largest and more consistent capacity factor values are located in all four corners of the island, southeast coast, and leeward side of the Ko'olau range (eastern part of the island). Both mountain ranges are characterized by favorable wind conditions but the complex terrain makes it likely impractical to develop wind farm infrastructure.

Regional climate models, including WRF, are very valuable tools to investigate the wind energy potential of complex terrain regions as shown by the model evaluation over Oahu. However, they also present some limitations that should not be disregarded and stem from factors such as the misrepresentation of sub-kilometer heterogeneities due to their spatial resolution, the Planetary Boundary Layer parameterization, differences between the estimated and the real response of the turbines to different wind regimes, and the use of wind profile approximations to compare with *in situ* observations among others. Addressing these aspects in the modeling system will likely improve wind energy estimates and are thus worth exploring in the future.

This study focused on physical aspects only to identify suitable regions for wind power resources and thus no political, environmental, or land management factors were considered despite their obvious importance.

Acknowledgements

We would like to acknowledge high-performance computing support from Yellowstone (ark:/85065/d7wd3xhc) provided by NCAR's Computational and Information Systems Laboratory, sponsored by the National Science Foundation. We would also like to thank the European Centre for Medium-Range Weather Forecast (ECMWF) for providing ERA-Interim Reanalysis data accessed through NCAR's Computational and Information Systems Laboratory. We also thank NCAR and other participating institutions for making WRF-ARW model available. This study was made possible in part by the data made available by governmental agencies, commercial firms, and educational institutions participating in MesoWest and wind farm data provided by the Hawaii Natural Energy Institute. This study was funded by the U.S. Department of Energy Cooperative Agreement DE-EE0003507; the Environmental Response, Energy and Food Security Tax; and the Office of Naval Research Award N00014-18-1-2166.

Appendix A. Supplementary data

Supplementary data related to this article can be found at https://doi.org/10.1016/j.renene.2018.05.080.

References

[1] U.S. Energy Information Administration, Net Generation by State by Type of Producer by Energy Source (EIA-906, EIA- 920, EIA-923), 1990-2014.
[2] U.S. Energy Information Administration, Rankings: Total Energy Consumed per Capita, 2014. http://www.eia.gov/state/rankings/?sid=US.
[3] J.E. Stopa, J.-F. Filipot, N. Li, K.F. Cheung, Y.-L. Chen, L. Vega, Wave energy resources along the Hawaiian Island chain, Renew. Energy 55 (2013) 305–321, https://doi.org/10.1016/j.renene.2012.12.030.
[4] D. Carvalho, A. Rocha, M. Gómez-Gesteira, C.S. Santos, WRF wind simulation and wind energy production estimates forced by different reanalyses: comparison with observed data for Portugal, Appl. Energy 117 (2014) 116–126, https://doi.org/10.1016/j.apenergy.2013.12.001.
[5] T.M. Giannaros, D. Melas, I. Ziomas, Performance evaluation of the Weather Research and Forecasting (WRF) model for assessing wind resource in Greece, Renew. Energy 102 (2017) 190–198, https://doi.org/10.1016/j.renene.2016.10.033.
[6] C. Mattar, D. Borvarán, Offshore wind power simulation by using WRF in the central coast of Chile, Renew. Energy 94 (2016) 22–31, https://doi.org/10.1016/j.renene.2016.03.005.
[7] P. Nolan, P. Lynch, C. Sweeney, Simulating the future wind energy resource of Ireland using the COSMO-CLM model, Wind Energy 17 (2012) 19–37, https://doi.org/10.1002/we.1554.
[8] C. Fant, C.A. Schlosser, K. Strzepek, The impact of climate change on wind and solar resources in southern Africa, Appl. Energy 161 (2016) 556–564, https://doi.org/10.1016/j.apenergy.2015.03.042.
[9] I. Tobin, S. Jerez, R. Vautard, F. Thais, E. van Meijgaard, A. Prein, et al., Climate change impacts on the power generation potential of a European mid-century wind farms scenario, Environ. Res. Lett. 11 (2016) 1–9, https://doi.org/10.1088/1748-9326/11/3/034013.
[10] S.D. Goddard, M.G. Genton, A.S. Hering, S.R. Sain, Evaluating the impacts of climate change on diurnal wind power cycles using multiple regional climate models, Environmetrics 26 (2015) 192–201, https://doi.org/10.1002/env.2329.
[11] Hawaiian Electric Companies (HECO), Hawaiian Electric Companies' Power Supply Improvement Plans Update Report: Book 2, 2016. http://cca.hawaii.gov/dca/hecos-psip-update-december-2016/.
[12] W.C. Skamarock, J.B. Klemp, J. Dudhia, D.O. Gill, D.M. Barker, M.G. Duda, et al., A Description of the Advanced Research WRF Version 3, NCAR/Tn-475+Str NCAR Technical Note, 2009, p. 125.
[13] C. Zhang, Y. Wang, A. Lauer, K. Hamilton, Configuration and evaluation of the WRF model for the study of Hawaiian regional climate, Mon. Weather Rev. 140 (2012) 3259–3277, https://doi.org/10.1175/MWR-D-11-00260.1.
[14] C. Zhang, Y. Wang, K. Hamilton, A. Lauer, Dynamical downscaling of the climate for the Hawaiian Islands. Part I: present day, J. Clim. 29 (2016) 3027–3048, https://doi.org/10.1175/JCLI-D-15-0432.1.
[15] P.A. Jiménez, J. Dudhia, J.F. González-Rouco, J.P. Montávez, E. García-Bustamante, J. Navarro, et al., An evaluation of WRF's ability to reproduce the surface wind over complex terrain based on typical circulation patterns, J. Geophys. Res. Atmos. 118 (2013) 7651–7669, https://doi.org/10.1002/jgrd.50585.
[16] D. Carvalho, A. Rocha, M. Gómez-Gesteira, C.S. Santos, Sensitivity of the WRF model wind simulation and wind energy production estimates to planetary boundary layer parameterizations for onshore and offshore areas in the Iberian Peninsula, Appl. Energy 135 (2014) 234–246, https://doi.org/10.1016/j.apenergy.2014.08.082.
[17] P.A. Jiménez, J. Dudhia, Improving the representation of resolved and unresolved topographic effects on surface wind in the WRF model, J. Appl. Meteorol. Climatol. 51 (2012) 300–316, https://doi.org/10.1175/JAMC-D-11-084.1.
[18] K. Horvath, D. Koracin, R. Vellore, J. Jiang, R. Belu, Sub-kilometer dynamical downscaling of near-surface winds in complex terrain using WRF and MM5 mesoscale models, J. Geophys. Res. Atmos. 117 (2012), D11111, https://doi.org/10.1029/2012JD017432.
[19] D. Carvalho, A. Rocha, M. Gómez-Gesteira, C.S. Santos, Offshore winds and wind energy production estimates derived from ASCAT, OSCAT, numerical weather prediction models and buoys—a comparative study for the Iberian Peninsula Atlantic coast, Renew. Energy 102 (2017) 433–444, https://doi.org/10.1016/j.renene.2016.10.063.
[20] N. Nawri, G.N. Petersen, H. Bjornsson, A.N. Hahmann, K. Jónasson, C.B. Hasager, et al., The wind energy potential of Iceland, Renew. Energy 69 (2014) 290–299, https://doi.org/10.1016/j.renene.2014.03.040.
[21] D.P. Dee, S.M. Uppala, A.J. Simmons, P. Berrisford, P. Poli, S. Kobayashi, et al., The ERA-Interim reanalysis: configuration and performance of the data assimilation system, Q. J. R. Meteorol. Soc. 137 (2011) 553–597, https://doi.org/10.1002/qj.828.
[22] H. von Storch, H. Langenberg, F. Feser, A spectral nudging technique for dynamical downscaling purposes, Mon. Weather Rev. 128 (2000) 3664–3673.
[23] H. Omrani, P. Drobinski, T. Dubos, Spectral nudging in regional climate modelling: how strongly should we nudge? Q. J. R. Meteorol. Soc. 138 (2012) 1808–1813, https://doi.org/10.1002/qj.1894.
[24] S.Y. Hong, Y. Noh, J. Dudhia, A new vertical diffusion package with an explicit treatment of entrainment processes, Mon. Weather Rev. 134 (2006) 2318–2341, https://doi.org/10.1175/MWR3199.1.
[25] S.Y. Hong, J. Lim, The WRF single-moment 6-class microphysics scheme (WSM6), J. Kor. Meteorol. Soc. 42 (2006) 129–151.
[26] Z. Guo, X. Xiao, Wind power assessment based on a WRF wind simulation with developed power curve modeling methods, Abstr. Appl. Anal. 2014 (2014) 1–15, https://doi.org/10.1155/2014/941648.
[27] F.J. Santos-Alamillos, D. Pozo-Vázquez, J.A. Ruiz-Arias, V. Lara-Fanego, J. Tovar-Pescador, Analysis of WRF model wind estimate sensitivity to physics parameterization choice and terrain representation in Andalusia (Southern Spain), J. Appl. Meteorol. Climatol. 52 (2013) 1592–1609, https://doi.org/10.1175/JAMC-D-12-0204.1.
[28] F. Chen, J. Dudhia, Coupling an advanced land surface–hydrology model with the Penn State–NCAR MM5 modeling system. Part I: model implementation

and sensitivity, Mon. Weather Rev. 129 (2001) 569–585, https://doi.org/10.1175/1520-0493(2001)129<0569:CAALSH>2.0.CO;2.
[29] E.W. Peterson, J.P. Hennessey Jr., On the use of power laws for estimates of wind power potential, J. Appl. Meteorol. 17 (1978) 390–394, https://doi.org/10.1175/1520-0450(1978)017<0390:OTUOPL>2.0.CO;2.
[30] J.A. Garza, P.-S. Chu, C.W. Norton, T.A. Schroeder, Changes of the prevailing trade winds over the islands of Hawaii and the North Pacific, J. Geophys. Res. 117 (2012), D11109, https://doi.org/10.1029/2011JD016888.
[31] J. Wang, J. Hu, K. Ma, Wind speed probability distribution estimation and wind energy assessment, Renew. Sustain. Energy Rev. 60 (2016) 881–899, https://doi.org/10.1016/j.rser.2016.01.057.
[32] J. King, A. Clifton, B.M. Hodge, Validation of Power Output for the WIND Toolkit, 2014. NREL/TP-5D00–61714.
[33] T.-J. Chang, C.-L. Chen, Y.-L. Tu, H.-T. Yeh, Y.-T. Wu, Evaluation of the climate change impact on wind resources in Taiwan Strait, Energy Convers. Manag. 95 (2015) 435–445, https://doi.org/10.1016/j.enconman.2015.02.033.